

NO-A179 891

HIGH TEMPERATURE OXIDATION AND ELECTROCHEMICAL STUDIES
RELATED TO HOT CORROSION(U) PENNSYLVANIA STATE UNIV
UNIVERSITY PARK DEPT OF MATERIALS SCI G SINKOVICH

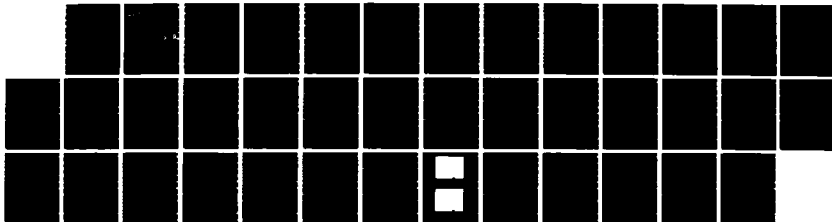
1/1

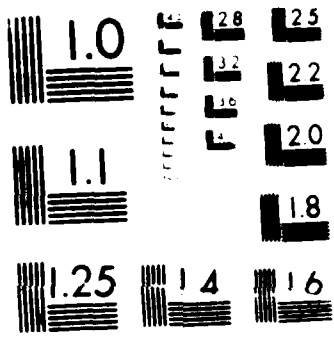
UNCLASSIFIED

APR 87 N00014-86-K-0133

F/G 7/4

NL





MICROCOPY RESOLUTION TEST CHART
NATIONAL BUREAU OF STANDARDS-1963-A

AD-A179 891

ANNUAL TECHNICAL REPORT

April 1987

OFFICE OF NAVAL RESEARCH

Contract No. N0014-86-K-0133

HIGH TEMPERATURE OXIDATION AND ELECTROCHEMICAL
STUDIES RELATED TO HOT CORROSION

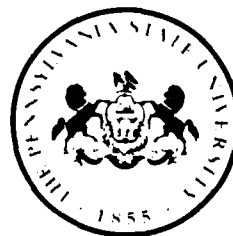
G. Simkovich

Department of Materials Science and Engineering
The Pennsylvania State University
University Park, Pennsylvania 16802

DTIC
SELECTED
APR 29 1987
S D
A

Reproduction in whole or in part is permitted for any purpose of the
United States Government. Distribution of this document is unlimited.

**The Pennsylvania
State University
University Park,
Pennsylvania**



THE PENNSYLVANIA STATE UNIVERSITY

College of Earth and Mineral Sciences

UNDERGRADUATE PROGRAMS OF STUDY

Ceramic Science and Engineering, Earth Sciences, Fuel Science, Geography, Geosciences, Metallurgy, Meteorology, Mineral Economics, Mining Engineering, Petroleum and Natural Gas Engineering, and Polymer Science.

GRADUATE PROGRAMS AND FIELDS OF RESEARCH

Ceramic Science, Fuel Science, Geochemistry and Mineralogy, Geography, Geology, Geophysics, Metallurgy, Meteorology, Mineral Economics, Mineral Processing, Mining Engineering, Petroleum and Natural Gas Engineering, and Polymer Science.

UNIVERSITY-WIDE INTERDISCIPLINARY GRADUATE PROGRAMS INVOLVING E&MS FACULTY AND STUDENTS

Earth Sciences, Ecology, Environmental Pollution Control Engineering, Mineral Engineering Management, Operations Research, Regional Planning, and Solid State Science.

ASSOCIATE DEGREE PROGRAMS

Metallurgical Engineering Technology and Mining Technology.

INTERDISCIPLINARY RESEARCH GROUPS WITHIN THE COLLEGE

Coal Research, Ore Deposits Research, Earth System Science, and the Mining and Mineral Resources Research Institute.

ANALYTICAL AND STRUCTURAL STUDIES

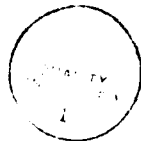
Classical chemical analysis of metals and silicate and carbonate rocks; X-ray crystallography; electron microscopy and diffraction; electron microprobe analysis; atomic absorption analysis; spectrochemical analysis; surface analysis by secondary ion mass spectrometry (SIMS); and scanning electron microscopy (SEM).

REPORT DOCUMENTATION PAGE		READ INSTRUCTIONS BEFORE COMPLETING FORM
1. REPORT NUMBER Annual Technical Report	2. GOVT ACCESSION NO. AD-A179891	3. RECIPIENT'S CATALOG NUMBER
4. TITLE (and Subtitle) High Temperature Oxidation and Electrochemical Studies Related to Hot Corrosion	5. TYPE OF REPORT & PERIOD COVERED Annual Technical Report	
	6. PERFORMING ORG. REPORT NUMBER	
7. AUTHOR(s) G. Simkovich	8. CONTRACT OR GRANT NUMBER(s) N0014-86-K-0133	
9. PERFORMING ORGANIZATION NAME AND ADDRESS Metallurgy Program, 209 Steidle Building The Pennsylvania State University University Park, PA 16802	10. PROGRAM ELEMENT, PROJECT, TASK AREA & WORK UNIT NUMBERS	
11. CONTROLLING OFFICE NAME AND ADDRESS Metallurgy Branch Office of Naval Research Arlington, CA 22217	12. REPORT DATE April 1987	
	13. NUMBER OF PAGES	
14. MONITORING AGENCY NAME & ADDRESS (if different from Controlling Office)	15. SECURITY CLASS. (of this report)	
	15a. DECLASSIFICATION/DOWNGRADING SCHEDULE	
16. DISTRIBUTION STATEMENT (of this Report)		
17. DISTRIBUTION STATEMENT (of the abstract entered in Block 20, if different from Report)		
18. SUPPLEMENTARY NOTES		
19. KEY WORDS (Continue on reverse side if necessary and identify by block number) SODIUM OXIDE NICKEL OXIDE SODIUM SULFATE		
20. ABSTRACT (Continue on reverse side if necessary and identify by block number) This report describes the 1st years efforts upon a number of processes related to hot corrosion. Total conductivities of pure Na_2SO_4 , Na_2SO_4 doped with NiO and Na_2SO_4 doped with Fe_2O_3 were measured at 900°C as a function of the activity of Na_2O . Partial electronic conductivities were also measured for the same systems utilizing the Wagner-Hebb type polarization cell. It was found that the total D.C. conductivity of pure Na_2SO_4 was of the order of $5 \times 10^{-2} \text{ (cm)}^{-1}$ and varied only slightly with changes in the activity of Na_2O .		

The partial conductivity of electrons in Na_2SO_4 was about two orders of magnitude less than the total conductivity while electron hole conductivities are considerably smaller than the electron conductivities. Thus, τ_e is of the order of 10^{-2} in pure Na_2SO_4 at 900°C .

The introduction of NiO and Fe_2O_3 into Na_2SO_4 at 900°C does not change significantly the total conductivities or the partial electronic conductivities except at a concentration of 10^{-2} mole % Fe_2O_3 where the electron and electron hole conductivities become of the same order of magnitude. At other concentrations of NiO and Fe_2O_3 the salt solution has electrons as a major minor carrier. This is somewhat surprising as one might generally anticipate an increase in the electron hole conduction with the introduction of multivalent ions of nickel and iron.

Hot corrosion studies on pure nickel under various heights of Na_2SO_4 were carried out at 900°C at $a_{\text{Na}_2\text{O}} = 6.3 \times 10^{-16}$. The kinetics of the hot corrosion process increased as the height of the Na_2SO_4 was increased from 0.5 cm to 2.0 cm. These results are quite informative in that they eliminate a number of possible reaction controlling steps. Further studies in this regime may aid in elucidating the reaction controlling step(s) for this process of hot corrosion.



Accession For	
NTIS CRA&I	<input checked="" type="checkbox"/>
DTIC TAB	<input type="checkbox"/>
Unannounced	<input type="checkbox"/>
Justification	
By	
Distribution /	
Availability Codes	
Dist	Avail and/or Special
A-1	

Introduction

The mechanism of hot corrosion is accepted as that of a dissolution process of protective oxides in a neighboring liquid phase, generally, but not always, considered to be Na_2SO_4 (other liquid salts create the same type of behavior). The reactions involved, considering only the formation of metal oxides, requires transport of oxygen through the liquid salt phase. Thus, at least in the initial stages of corrosion, one of the interface reactions and/or diffusion in the boundary layers and/or diffusion through the bulk salt must control the process. After a certain thickness of reaction product accumulates at the liquid-alloy interface it is then logical to anticipate control of the corrosion process to be reactions that involve this scale.

To aid in the overall understanding of the hot corrosion process determination of a number of electrical transport processes in the Na_2SO_4 phase have been undertaken. The experiments conducted are described in the following text and the experimental results obtained during the first year of study are presented.

Experimental

A variety of electrical transport experiments were conducted. These include the measurement of the total electrical conductivity of pure Na_2SO_4 at 900°C under various $\text{SO}_2 + \text{O}_2$ atmospheres and determination of the partial conductivities of electrons and electron holes utilizing a Wagner-Hebb type polarization cell for pure and "doped" Na_2SO_4 also at 900°C under $\text{SO}_2 + \text{O}_2$ atmospheres of various concentrations.

The crucible utilized for these experiments was pure gold which is relatively inert to the aggressive salt. Gold electrodes were also employed. Atmospheres of $\text{SO}_2 + \text{O}_2$ employed to vary the activity of the Na_2O in the melt

were obtained from gas mixtures or by flowing an inert gas, He, over $ZnSO_4/ZnO$ mixtures held at a constant temperature in a furnace separate from the cell furnace. A platinum wire screen placed above the melt was utilized to catalyze the reaction. Both D.C. and A.C. measurements were made but most of the work reported herein relate to D.C. measurements since these appeared to be most stable and reproducible.

The cell constant was obtained by measuring a standard KCl solution at room temperature under identical conditions to those utilized for the cell at the high temperature operation.

In addition to the above electrochemical measurements high temperature, $900^\circ C$, hot corrosion studies were begun on metal samples covered by a certain thickness of liquid Na_2SO_4 . The initial experiments were carried out in silica crucibles with pure nickel as the metal phase. The nickel was oxidized at $1000^\circ C$ for about 12 hours. One surface of the oxidized sample was polished to obtain a clean metal surface while the other surfaces were permitted to retain their oxide layer. The oxide surfaces were then coated with a thin gold layer in order to protect these surfaces from reaction with the Na_2SO_4 .

Weight changes during the hot corrosive process were followed by an automatic recording balance. The activity of Na_2O was maintained at about 6.3×10^{-16} by a flowing gas stream of $O_2 + SO_2$.

Results and Discussion

Electrical Conductivities

The total electrical conductivity of pure Na_2SO_4 as a function of the activity of Na_2O in the melt at 1173 K is depicted in Figure 1. The conductivities at 100 and 1000 Hz differ from the D.C. values obtained indicating that polarization may be present at the electrodes. However, the

A.C. values measured were not nearly as stable or reproducible as the D.C. values. Hence, at this time we relate our subsequent calculations to the total D.C. conductivities. Figure (1a) displays this conductivity on a more sensitive conductivity scale. From this figure one notes a small but definite decrease in the conductivity as the activity of the Na_2O decreases. We are presently giving thought to this decrease in order to attempt an explanation of the observed trend.

From Wagner-Hebb types of polarization measurements on pure Na_2SO_4 at 1173 K the partial conductivities of electrons and electron holes were calculated and are depicted in Figure 2. It can be seen that electron conduction in pure Na_2SO_4 is considerably larger than that of electron holes. Thus, for pure Na_2SO_4 the major minor conductors are electrons. The calculated transport number of the electronic species are depicted in Figure 3 from which it can be seen that electron transport numbers are of the order of 10^{-2} while that of the electron holes are of the order of $1-2 \times 10^{-4}$. Thus, a relatively large amount of the transport of charge is electronic in nature in pure Na_2SO_4 , i.e. of the order of 1 part in a hundred parts. The transport numbers of electronic species in molten salts have not been measured to any great extent but the few that have been measured are smaller than that determined in this study, e.g. reference 1 gives a value of about 3×10^{-3} for electrons in the molten eutectic of LiCl-KCl at 450°C .

In view of the fact that nickel based alloys are frequently utilized for applications (2-11) where hot corrosion may occur electrical conductivities and Wagner-Hebb type polarization measurements of Na_2SO_4 with additions of NiO have been made. The total conductivities of these melts are depicted in Figure 4 along with that of pure Na_2SO_4 . It should be noted that the 10 mole % NiO solution is in excess of the solubility limits as determined by Gupta and Rapp

(12) except for the extreme ends of the activities of Na_2SO_4 ; thus, the central section of this conductivity curve represents the ionic solution conductivity plus the contribution, if any, of the suspended solid phase. The conductivity scale utilized in Figure 4 is rather amplified so that the trends of the conductivities may be observed.

From these results one notes that there is no "massive" change of conductivities of NiO "doped" Na_2SO_4 as compared to pure Na_2SO_4 . Of course, the levels of NiO additions are not excessive, except for the 10 mole % NiO case, so that major changes in total conductivities are not expected. However, there is a trend in the conductivities to minimize in the neighborhood of $a_{\text{Na}_2\text{O}} = 10^{-8}$ to 10^{-10} . This is in the neutral region between acid and basic fluxing of the NiO and is similar to the solubility curve of NiO determined by Gupta and Rapp (12).

In general, one may note that the results obtained do indicate that the mobilities of the ions resulting from the dissolution of NiO are not significantly different from the ions present in the Na_2SO_4 melt.

The partial electronic conductivities observed for the NiO doped Na_2SO_4 are depicted in Figures 5 to 7. These have been plotted as separate figures since a single figure plot would show much intermixing of values. Basically, these results show that electron conductivities remain higher than the electron hole conductivities at all concentrations of NiO and throughout the entire range of Na_2O activities. This is somewhat surprising since one would anticipate that the introduction of nickel ions into the melt would tend to increase the electron hole conduction via the exchange of electrons between Ni^{2+} and Ni^{3+} ions. Such apparently does not occur and the postulate that the presence of nickel in Na_2SO_4 solutions would enhance the total electronic conductivity and more specifically the electron hole conduction is certainly not in accord with these results.

Utilizing the total conductivities and the partial conductivities one may calculate the transport numbers of the electronic species in these doped solutions. These values are plotted in Figures 8 to 10. It can be seen that the electron transport numbers remain consistently higher than those of the electron holes in accord with the partial and total conductivities depicted previously. Again, the effect of the dissolution of the NiO is minimal upon the electron hole transport.

The effect of Fe_2O_3 dissolved in Na_2SO_4 was also studied. Figure 11 depicts the total conductivities at various concentrations of Fe_2O_3 while Figures 12 to 14 depict the partial electronic conductivities. Electron conductivities are considerably higher as compared to electron hole conductivities except for the 10^{-2} mol % Fe_2O_3 concentration. This is seen more clearly in Figures 15 to 17 which show the calculated transport numbers of these solutions. It is noted that at relatively low activities of Na_2O (10^{-14} - 10^{-15}) that the electron conductivity is considerably enhanced as compared to higher activities indicating that the concentration and/or mobilities of the electrons is increased significantly in this activity region. Indeed, the total conductivities, Figure 11, are also increased considerably in this region indicating that both ionic and electronic transport are enhanced. Such may relate to dissolution products of the Fe_2O_3 in the Na_2SO_4 melt.

The above represents at this point in time the electrochemical results obtained. Interpretation(s) of these results are presently under consideration.

Hot Corrosion of Pure Ni as a Function of Na_2SO_4 Height

As noted in the experimental section of this report nickel samples, prepared to expose one metallic surface to an overlying Na_2SO_4 melt, were tested at 900°C at an activity of Na_2O of about 6.3×10^{-16} . The results obtained are

shown in Figure 18. It can be seen that the gain in weight per unit area of sample increases as the height of the melt above the metal increases. Thus, diffusion through the entire distance of the overlying Na_2SO_4 is not rate determining for this corrosion process.

Figure 19 shows a typical SEM micrograph of the layers formed on the nickel under the conditions of the experiment. Both NiO and Ni_3S_2 are present in a duplex type scale indicating that the sulfur potential is sufficient at the scale - Na_2SO_4 interface to form the Ni_3S_2 even though the gaseous atmosphere is such so as to establish an acid fluxing Na_2SO_4 melt. Figure 20 is an x-ray map of the micrograph shown in Figure 19 and reveals the distribution of the sulfur in the various phases present. Again, it is apparent that the central structure is a high sulfur containing compound.

The differences seen in weight gain as a function of height of Na_2SO_4 are worthy of further discussion. If one considers the possible rate controlling steps in this process and considers whether the step is altered by the height of the Na_2SO_4 layer one is led to the following conclusions:

<u>Step</u>	Effect of a thicker Na_2SO_4 layer
1. Diffusion flux through the Na_2SO_4 thickness	Decrease
2. Diffusion flux through boundary layer at gas - Na_2SO_4 interface	No change, essentially
3. Diffusion flux through boundary layer at scale - Na_2SO_4 interface	No change, essentially (see further discussion)
4. Interface reaction at the gas - Na_2SO_4 interface	No change, essentially
5. Interface reaction at the Na_2SO_4 - scale interface	No change, essentially (see further discussion)
6. Oxidizing potential gradient from gas - Na_2SO_4 interface to scale - Na_2SO_4 interface	Decrease

References

1. J. R. Durst and R. A. Rapp, *J. Electrochem. Soc.*, **127**, 2194-2656 (1980).
2. J. R. Durst and R. A. Rapp, *J. Electrochem. Soc.*, **127**, 2194-2656 (1980).
3. J. R. Durst and R. A. Rapp, *J. Electrochem. Soc.*, **127**, 2194-2656 (1980).
4. J. R. Durst and R. A. Rapp, *J. Electrochem. Soc.*, **127**, 2194-2656 (1980).
5. J. R. Durst and R. A. Rapp, *J. Electrochem. Soc.*, **127**, 2194-2656 (1980).
6. J. R. Durst and R. A. Rapp, *J. Electrochem. Soc.*, **127**, 2194-2656 (1980).
7. J. R. Durst and R. A. Rapp, *J. Electrochem. Soc.*, **127**, 2194-2656 (1980).
8. J. R. Durst and R. A. Rapp, *J. Electrochem. Soc.*, **127**, 2194-2656 (1980).
9. J. R. Durst and R. A. Rapp, *J. Electrochem. Soc.*, **127**, 2194-2656 (1980).
10. J. R. Durst and R. A. Rapp, *J. Electrochem. Soc.*, **127**, 2194-2656 (1980).
11. J. R. Durst and R. A. Rapp, *J. Electrochem. Soc.*, **127**, 2194-2656 (1980).
12. J. R. Durst and R. A. Rapp, *J. Electrochem. Soc.*, **127**, 2194-2656 (1980).
13. J. R. Durst and R. A. Rapp, *J. Electrochem. Soc.*, **127**, 2194-2656 (1980).
14. J. R. Durst and R. A. Rapp, *J. Electrochem. Soc.*, **127**, 2194-2656 (1980).
15. J. R. Durst and R. A. Rapp, *J. Electrochem. Soc.*, **127**, 2194-2656 (1980).
16. J. R. Durst and R. A. Rapp, *J. Electrochem. Soc.*, **127**, 2194-2656 (1980).
17. J. R. Durst and R. A. Rapp, *J. Electrochem. Soc.*, **127**, 2194-2656 (1980).
18. J. R. Durst and R. A. Rapp, *J. Electrochem. Soc.*, **127**, 2194-2656 (1980).
19. J. R. Durst and R. A. Rapp, *J. Electrochem. Soc.*, **127**, 2194-2656 (1980).
20. J. R. Durst and R. A. Rapp, *J. Electrochem. Soc.*, **127**, 2194-2656 (1980).

List of Figures

- Figure 1. Log (conductivity) versus Na_2O activity in a pure Na_2SO_4 melt as a function of frequency at 1173 K.
- Figure 1a. D.C. Conductivity versus Na_2O activity in a pure Na_2SO_4 melt at 1173 K.
- Figure 2. Electronic conductivities in a pure Na_2SO_4 melt as a function of Na_2O activity at 1173 K.
- Figure 3. Transport numbers of electronic species in a pure Na_2SO_4 melt at 1173 K.
- Figure 4. Total conductivities versus Na_2O activity in a Na_2SO_4 melt with different concentrations of NiO at 1173 K.
- Figure 5. Partial electronic conductivities in a Na_2SO_4 melt with the addition of 10^{-3} m/o NiO as a function of Na_2O activity at 1173 K.
- Figure 6. Partial electronic conductivities in molten Na_2SO_4 with the addition of 1.8×10^{-1} m/o NiO as a function of Na_2O activity at 1173 K.
- Figure 7. Partial electronic conductivities in molten Na_2SO_4 with supersaturated NiO (10 m/o) as a function of Na_2O activity at 1173 K.
- Figure 8. Transport numbers of electronic species in molten Na_2SO_4 containing 10^{-3} m/o NiO at 1173 K.
- Figure 9. Transport numbers of electronic species in molten Na_2SO_4 with 1.8×10^{-1} m/o NiO as a function of Na_2O activity at 1173 K.
- Figure 10. Transport numbers of electronic species in molten Na_2SO_4 with supersaturated NiO (10 m/o) as a function of Na_2O activity at 1173 K.
- Figure 11. Total conductivities of molten Na_2SO_4 with different concentrations of $\alpha\text{-Fe}_2\text{O}_3$ as a function of sodium oxide activity at 1173 K.
- Figure 12. Partial electronic conductivities in a Na_2SO_4 melt containing 10^{-3} m/o $\alpha\text{-Fe}_2\text{O}_3$ as a function of Na_2O activity at 1173 K.
- Figure 13. Partial electronic conductivities in Na_2SO_4 melt containing 10^{-2} m/o $\alpha\text{-Fe}_2\text{O}_3$ as a function of Na_2O activity at 1173 K.
- Figure 14. Partial electronic conductivities in a Na_2SO_4 melt containing supersaturated $\alpha\text{-Fe}_2\text{O}_3$ (1 m/o) as a function of Na_2O activity at 1173 K.
- Figure 15. Transport numbers of electronic species in molten Na_2SO_4 with 10^{-3} m/o $\alpha\text{-Fe}_2\text{O}_3$ as a function of Na_2O activity at 1173 K.

Figure 16. Transport numbers of electronic species in molten Na_2SO_4 with 10^{-2} m/o $\alpha\text{-Fe}_2\text{O}_3$ as a function of Na_2O activity at 1173 K.

Figure 17. Transport numbers of electronic species in molten Na_2SO_4 with supersaturated $\alpha\text{-Fe}_2\text{O}_3$ (1 m/o) as a function of Na_2O activity at 1173 K.

Figure 18. Weight gain vs. time as a function of Na_2SO_4 level.

Figure 19. Ni_3S_2 deposit located beneath dense NiO scale.

Figure 20. X-ray mapping of the distribution of sulfur.

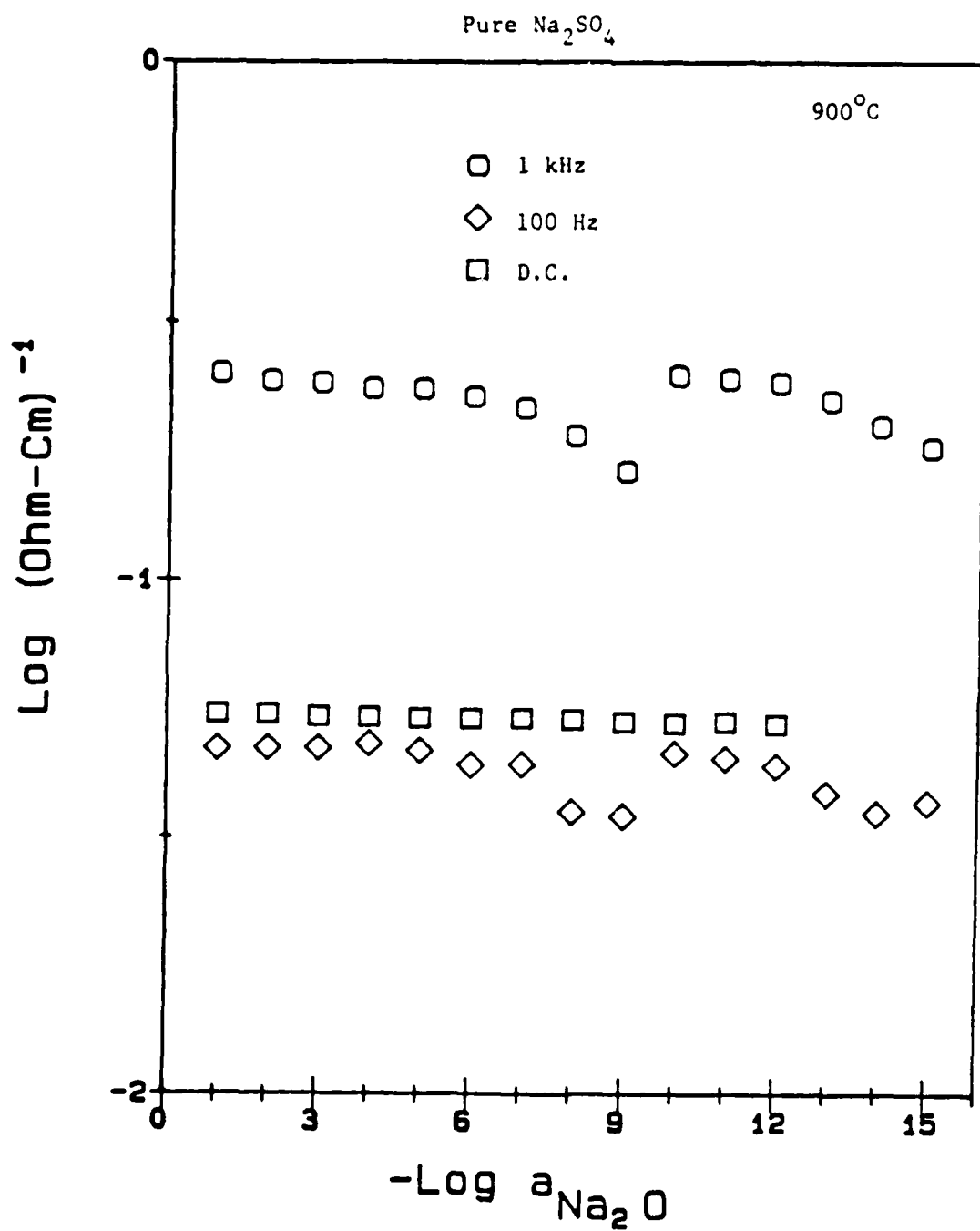


Figure 1. Log (conductivity) versus Na₂O activity in a pure Na₂SO₄ melt as a function of frequency at 1173K

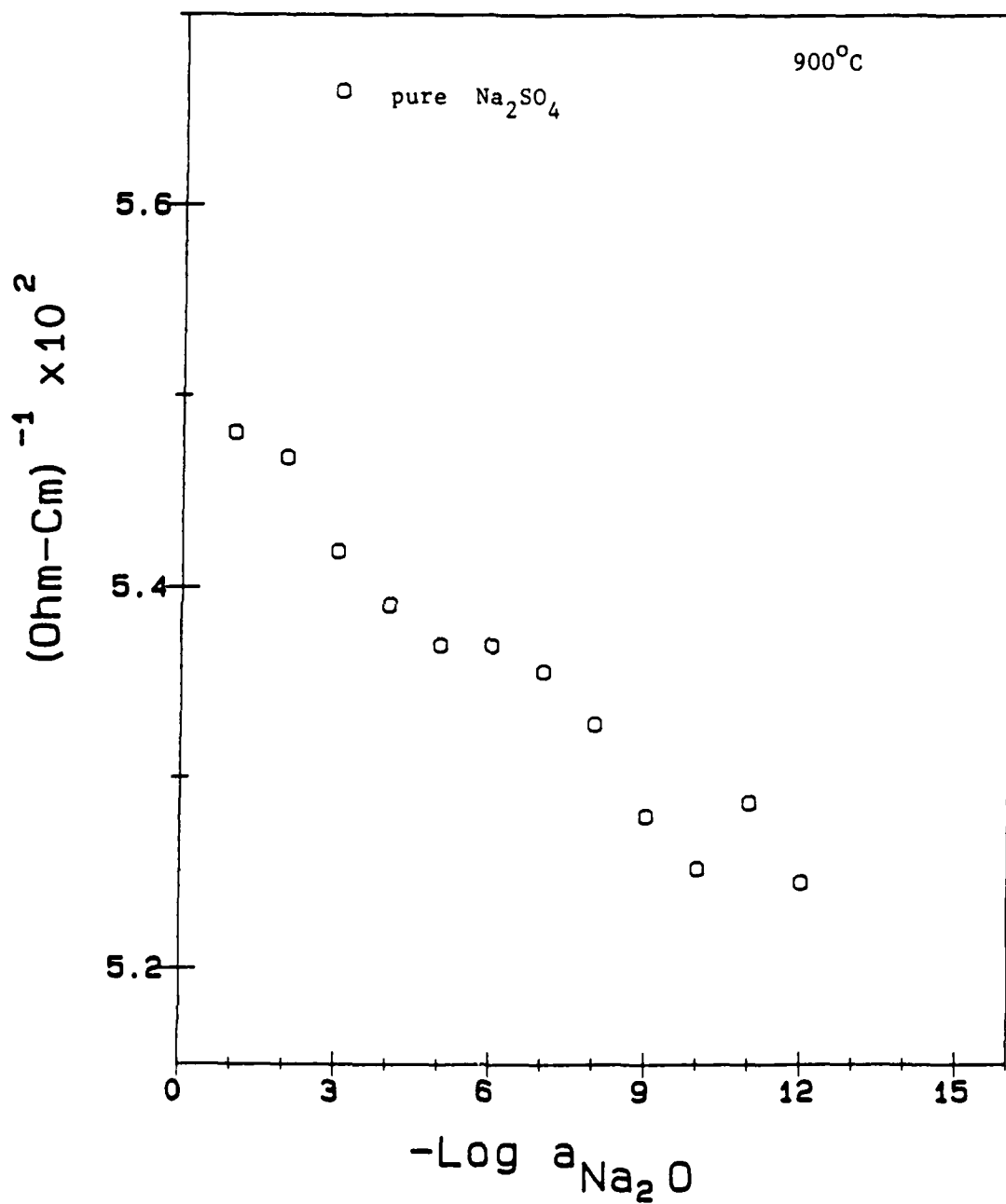


Figure 1.(a). D.C. Conductivity versus Na₂O activity in a pure Na₂SO₄ melt at 1173 K

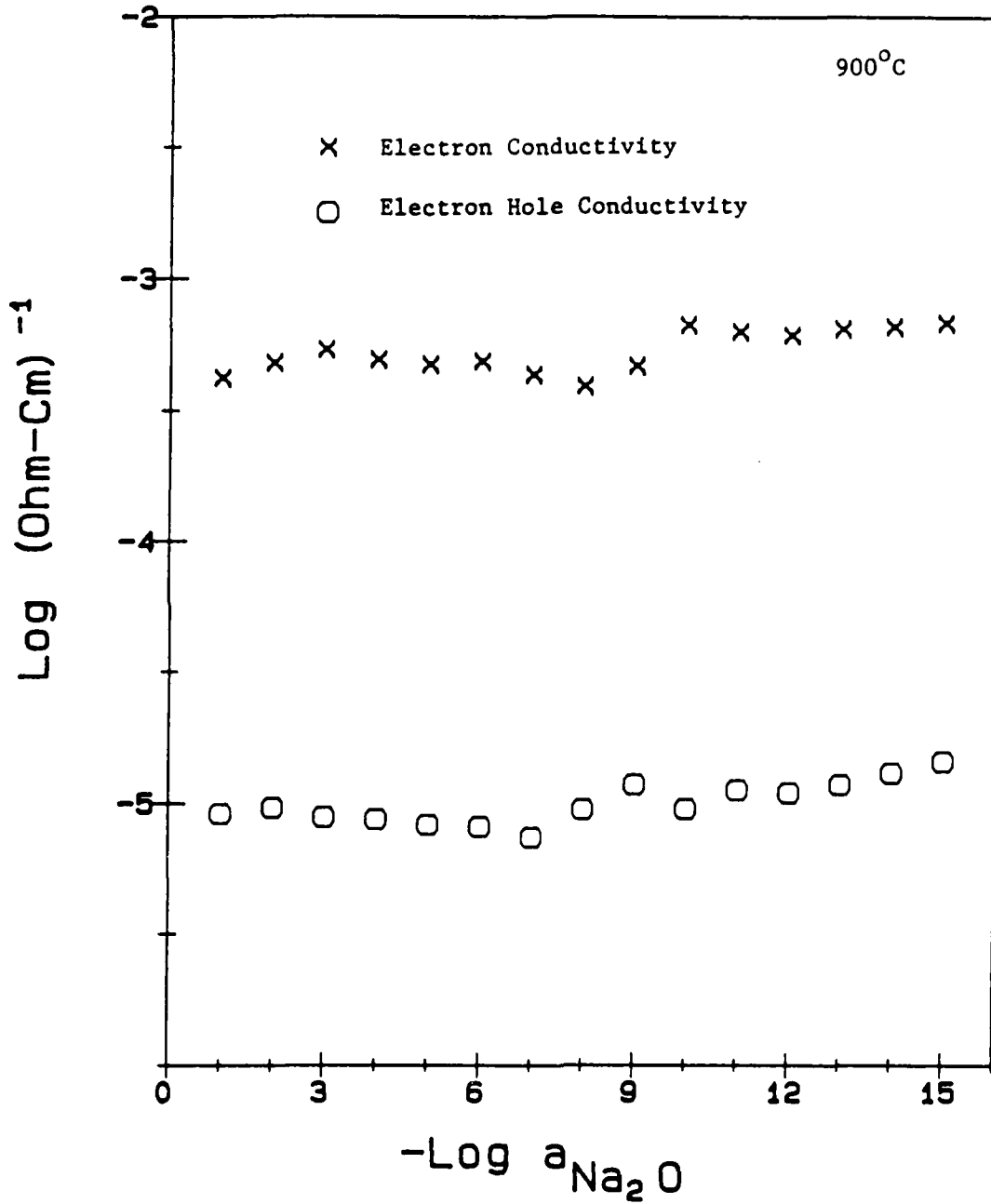


Figure 2. Electronic conductivities in a pure Na₂SO₄ melt as a function of Na₂O activity at 1173 K

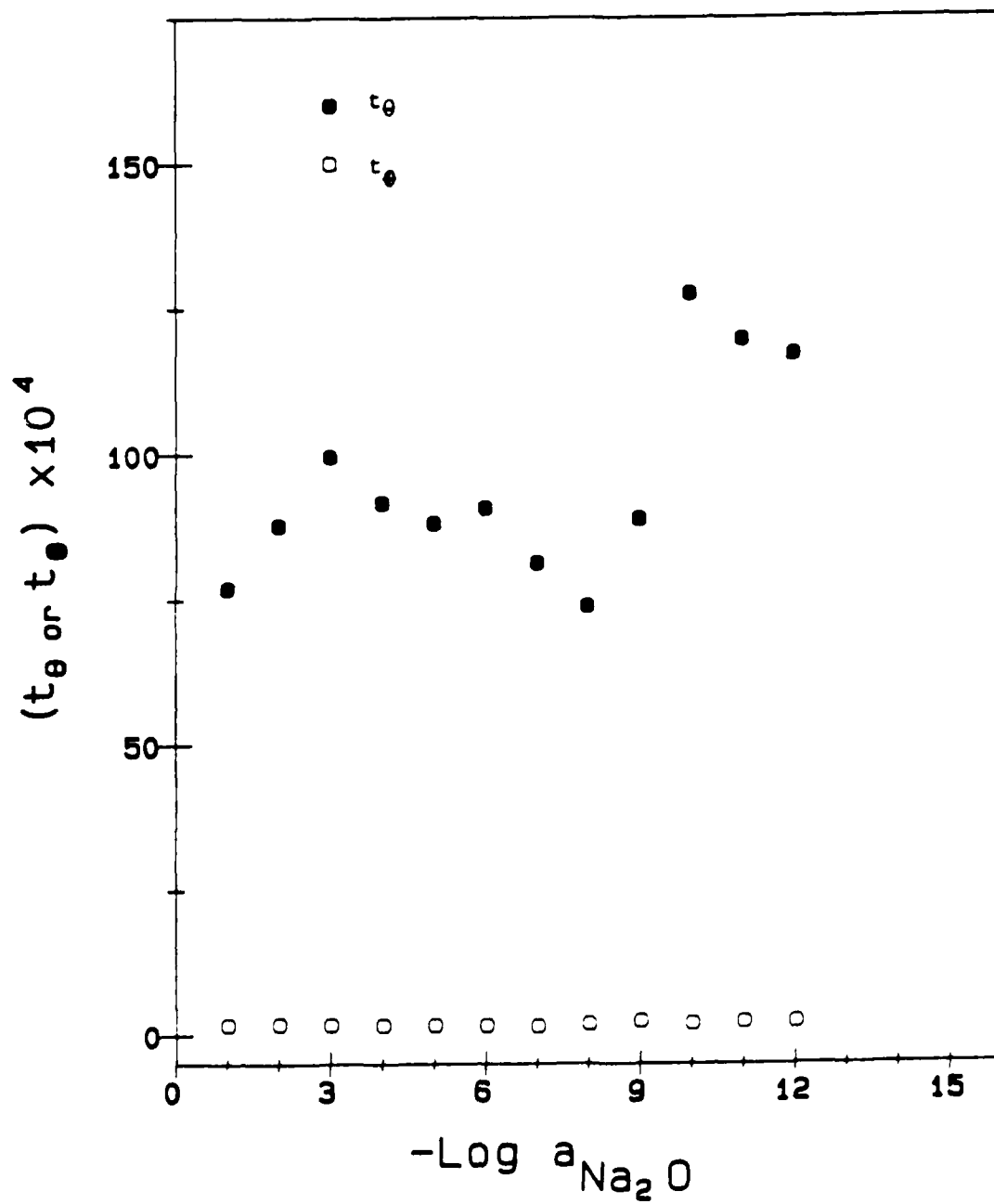


Figure 3. Transport numbers of electronic species in a pure Na₂SO₄ melt at 1173 K

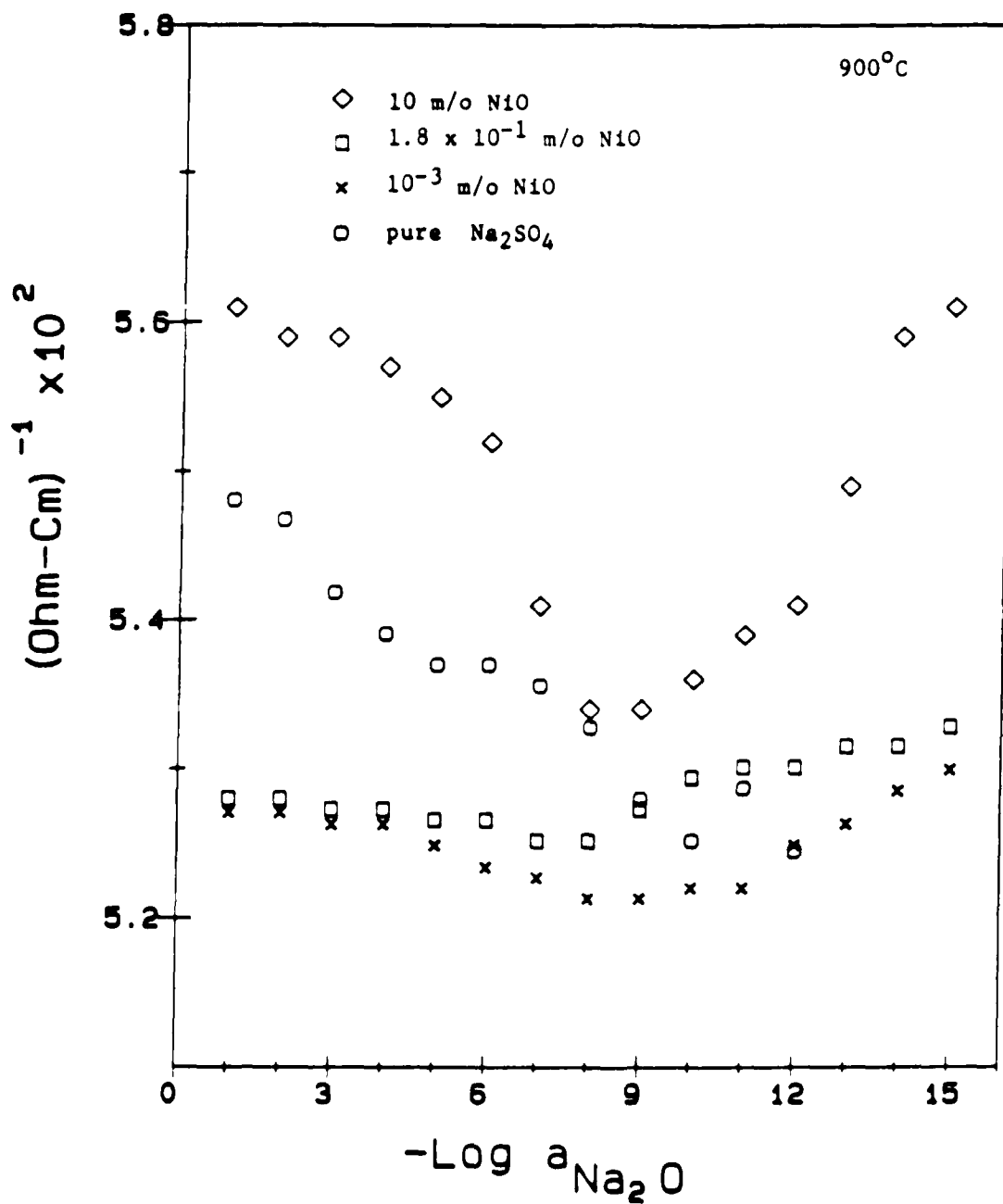


Figure 4. Total conductivities versus Na₂O activity in a Na₂SO₄ melt with different concentrations of NiO activity at 1173 K

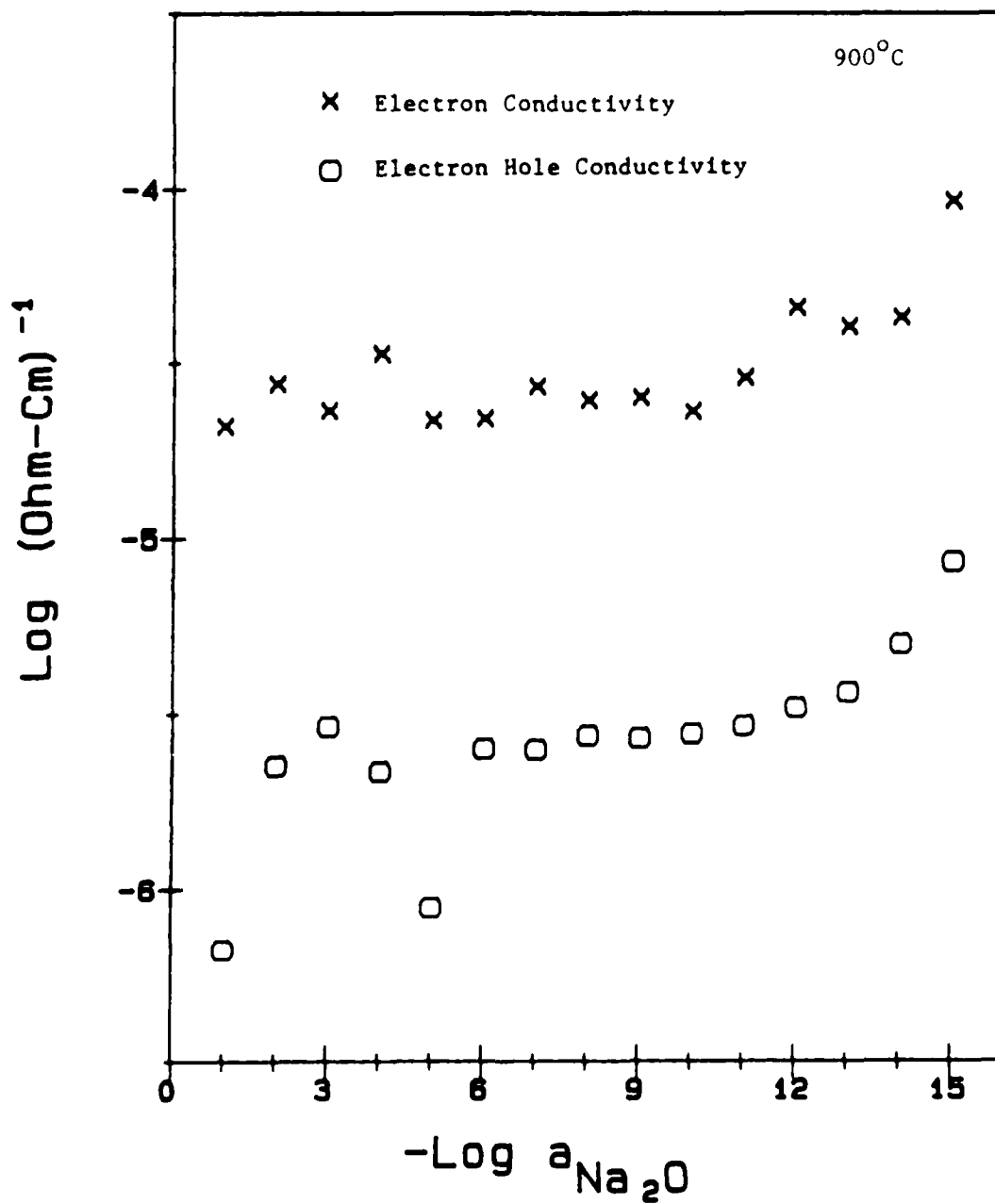


Figure 5. Partial electronic conductivities in a Na₂SO₄ melt with the addition of 10⁻³ m/o NiO as a function of Na₂O activity at 1173 K

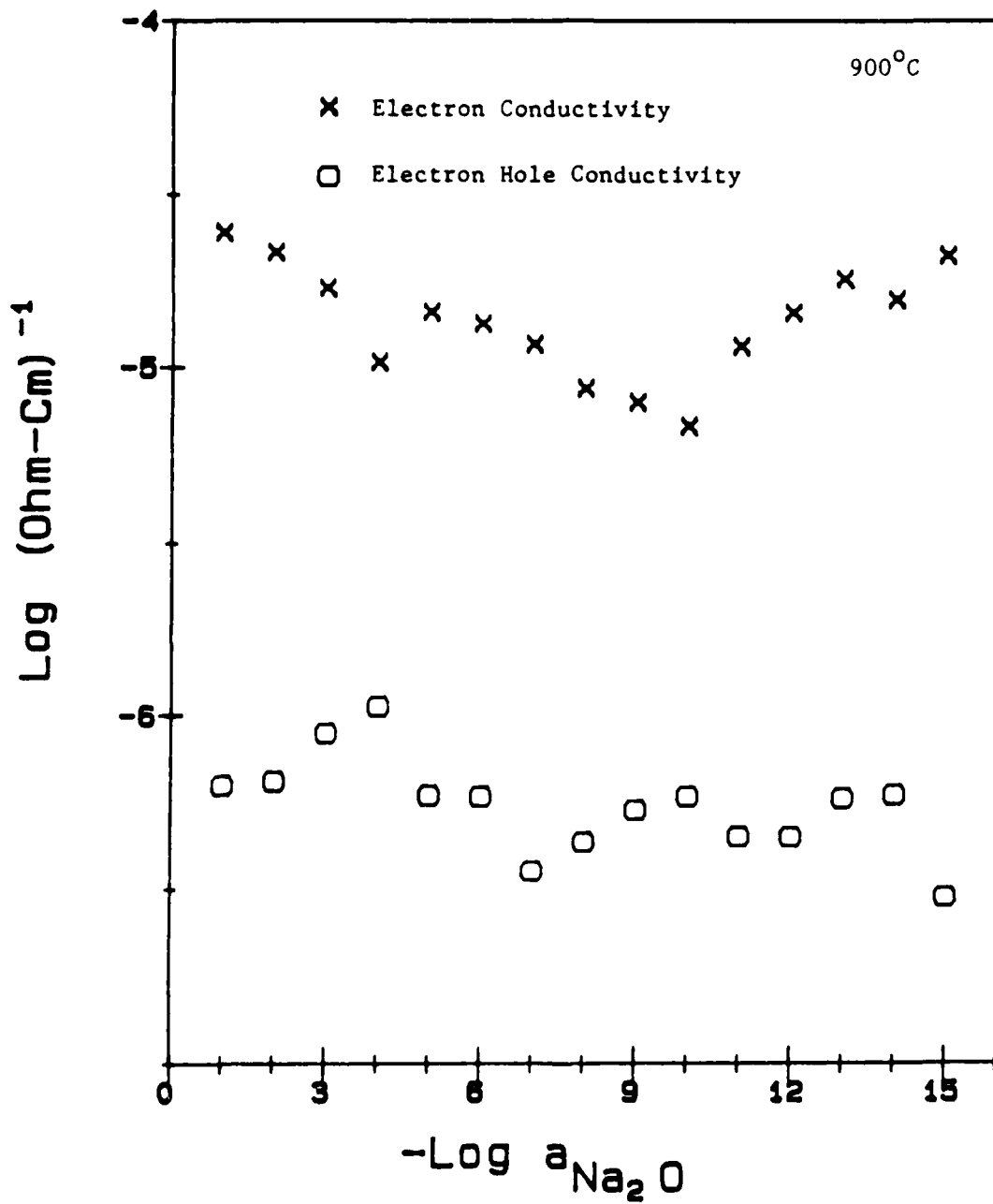


Figure 6. Partial electronic conductivities in molten Na₂SO₄ with the addition of 1.8 x 10⁻¹ m/o NiO as a function of Na₂O activity at 1173 K

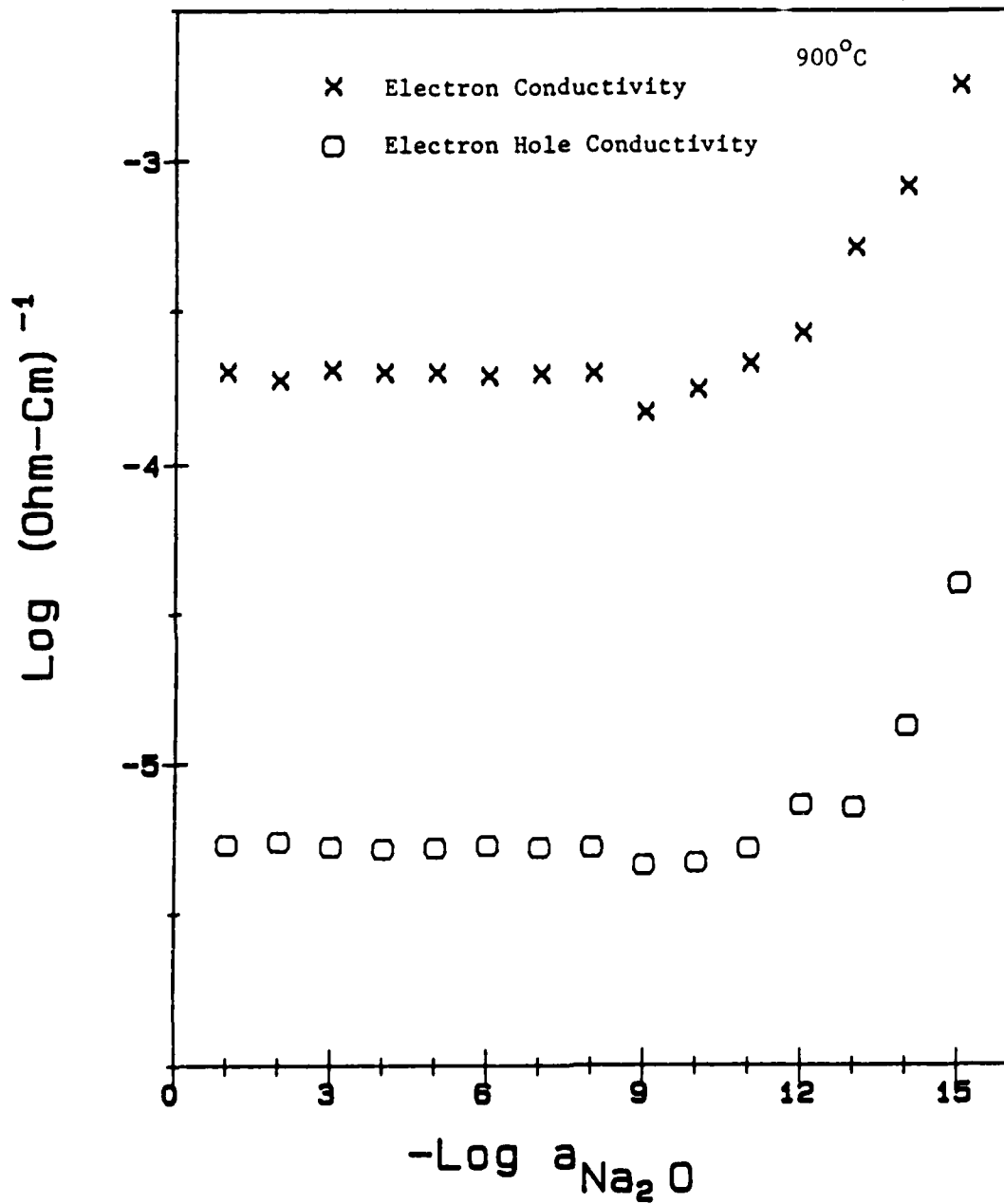


Figure 7. Partial electronic conductivities in molten Na₂SO₄ with supersaturated NiO (10 m/o) as a function of Na₂O activity at 1173 K

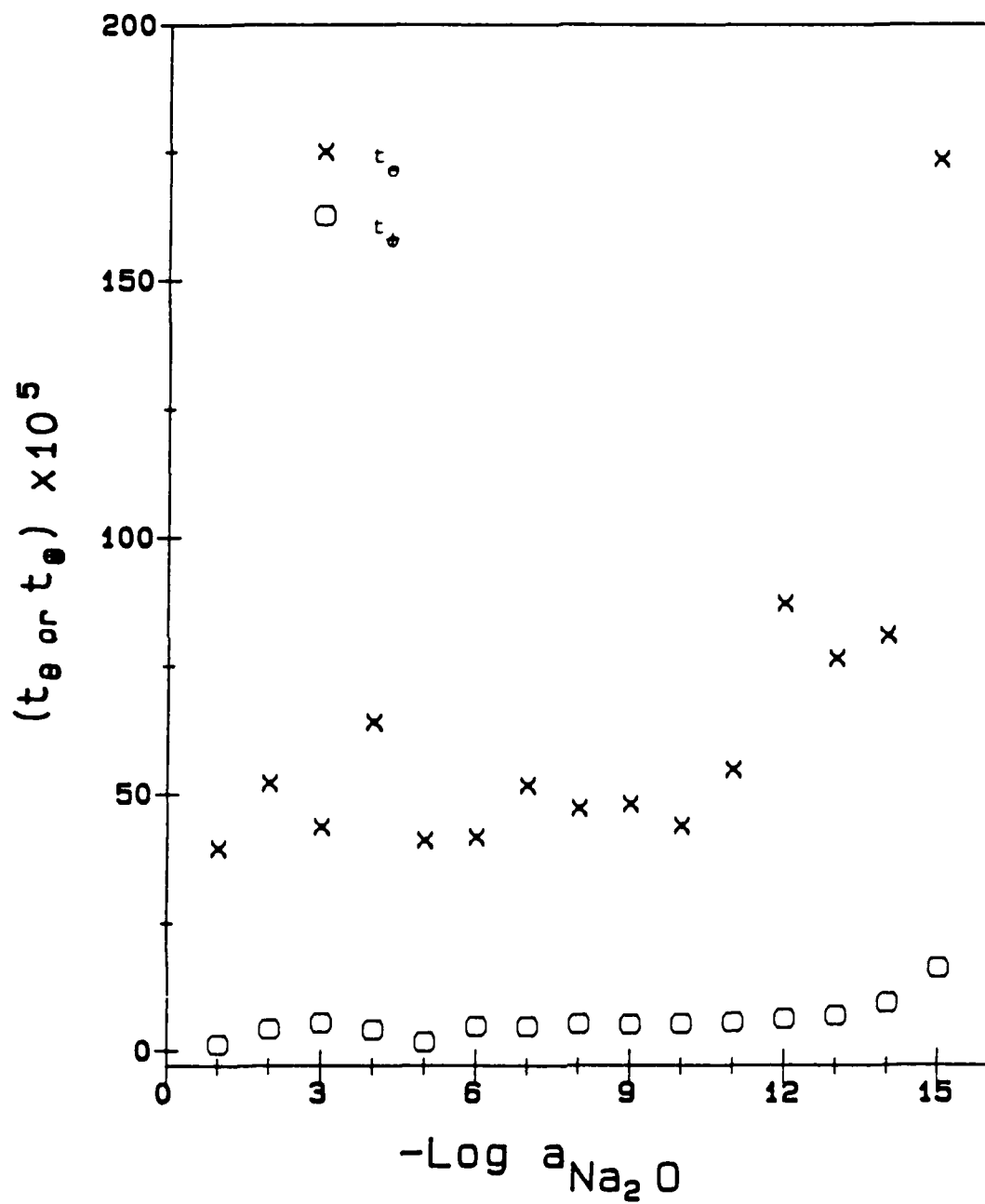


Figure 8. Transport numbers of electronic species in molten Na₂SO₄ containing 10⁻³ m/o NiO at 1173 K

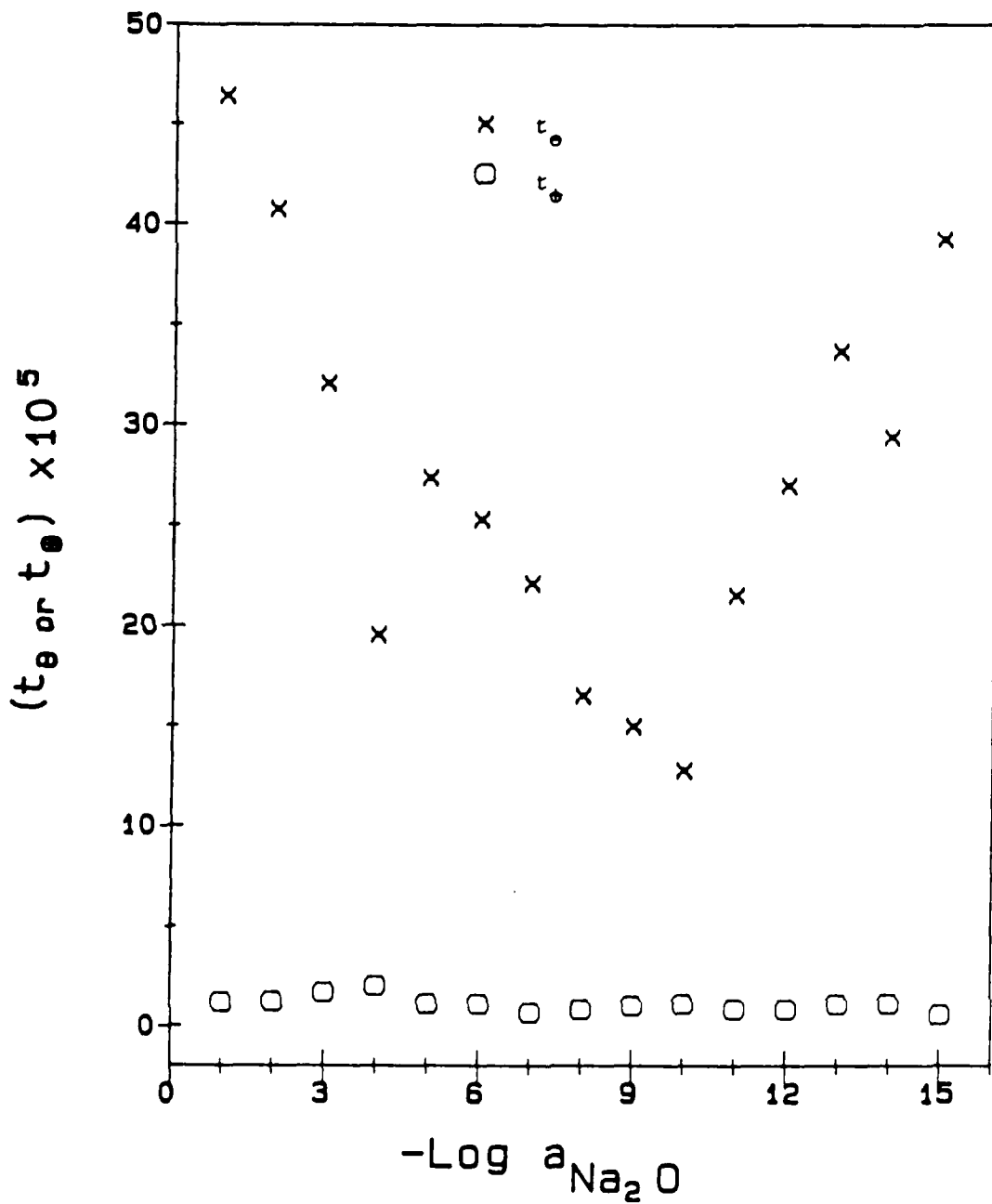


Figure 9. Transport numbers of electronic species in molten Na₂SO₄ with 1.8 x 10⁻¹ m/o NiO as a function of Na₂O activity at 1173 K

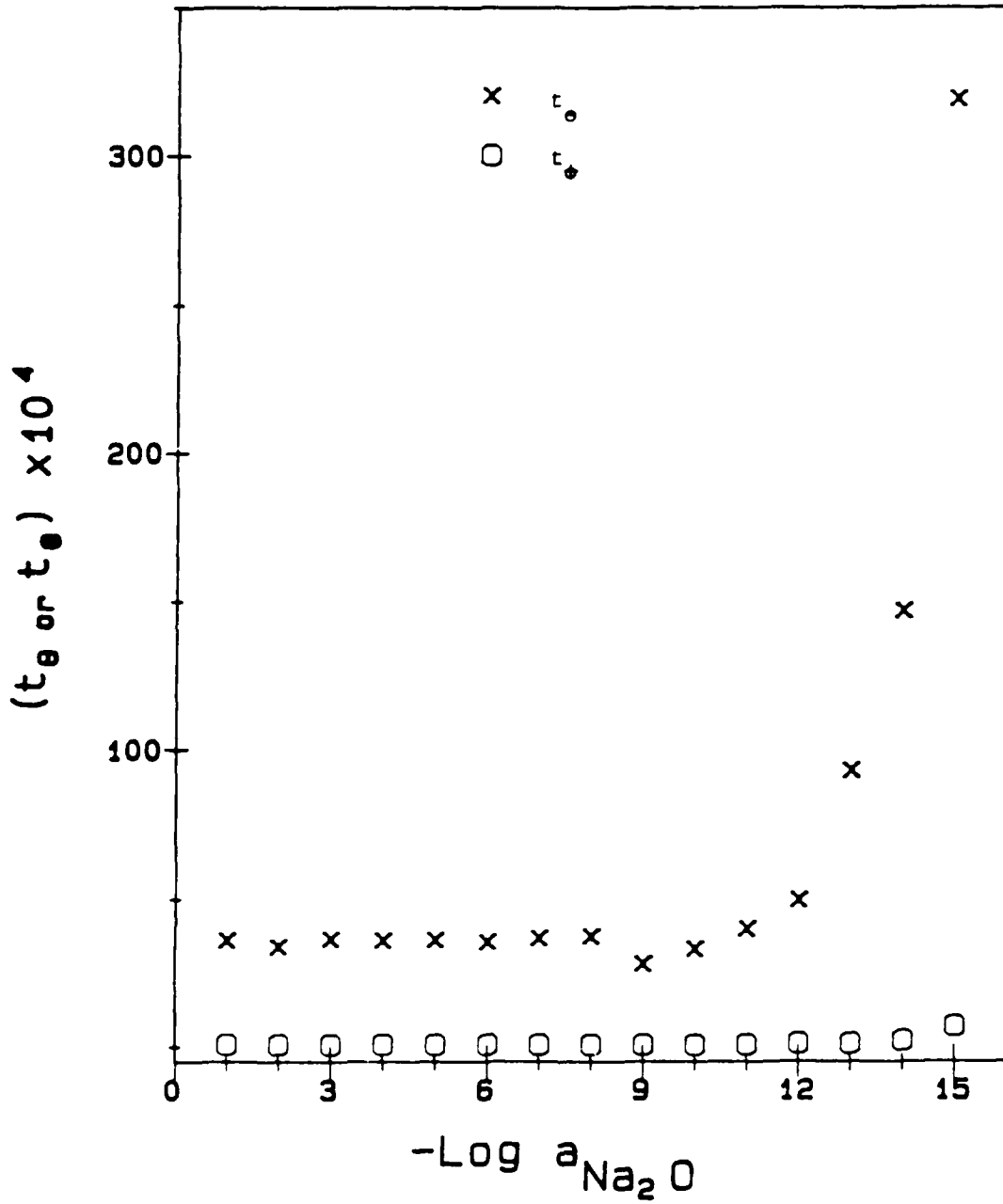


Figure 10. Transport numbers of electronic species in molten Na_2SO_4 with supersaturated NiO (10 m/o) as a function of Na_2O activity at 1173 K

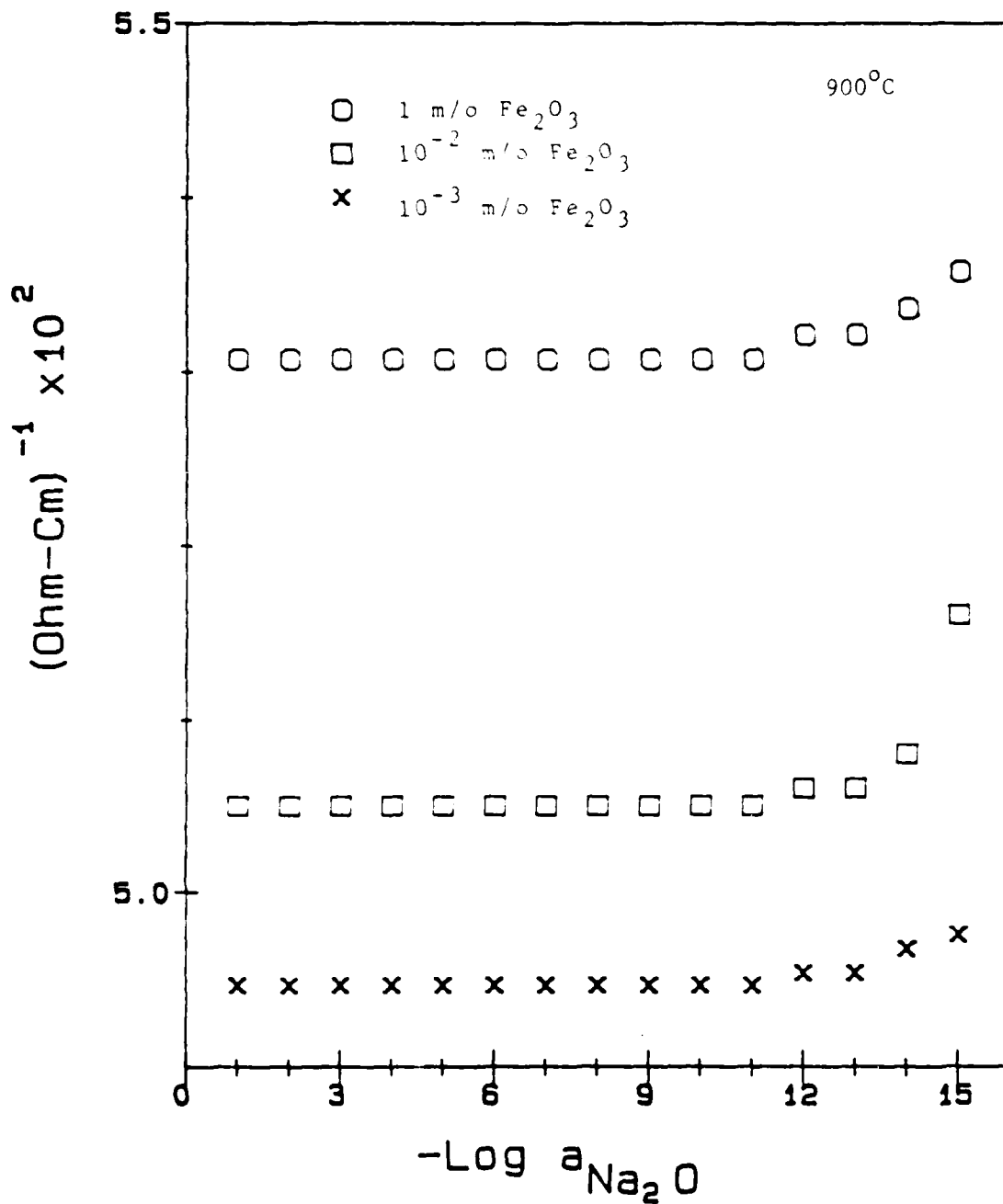


Figure 11. Total conductivities of molten Na₂SO₄ with different concentrations of α-Fe₂O₃ as a function of sodium oxide activity at 1173 K

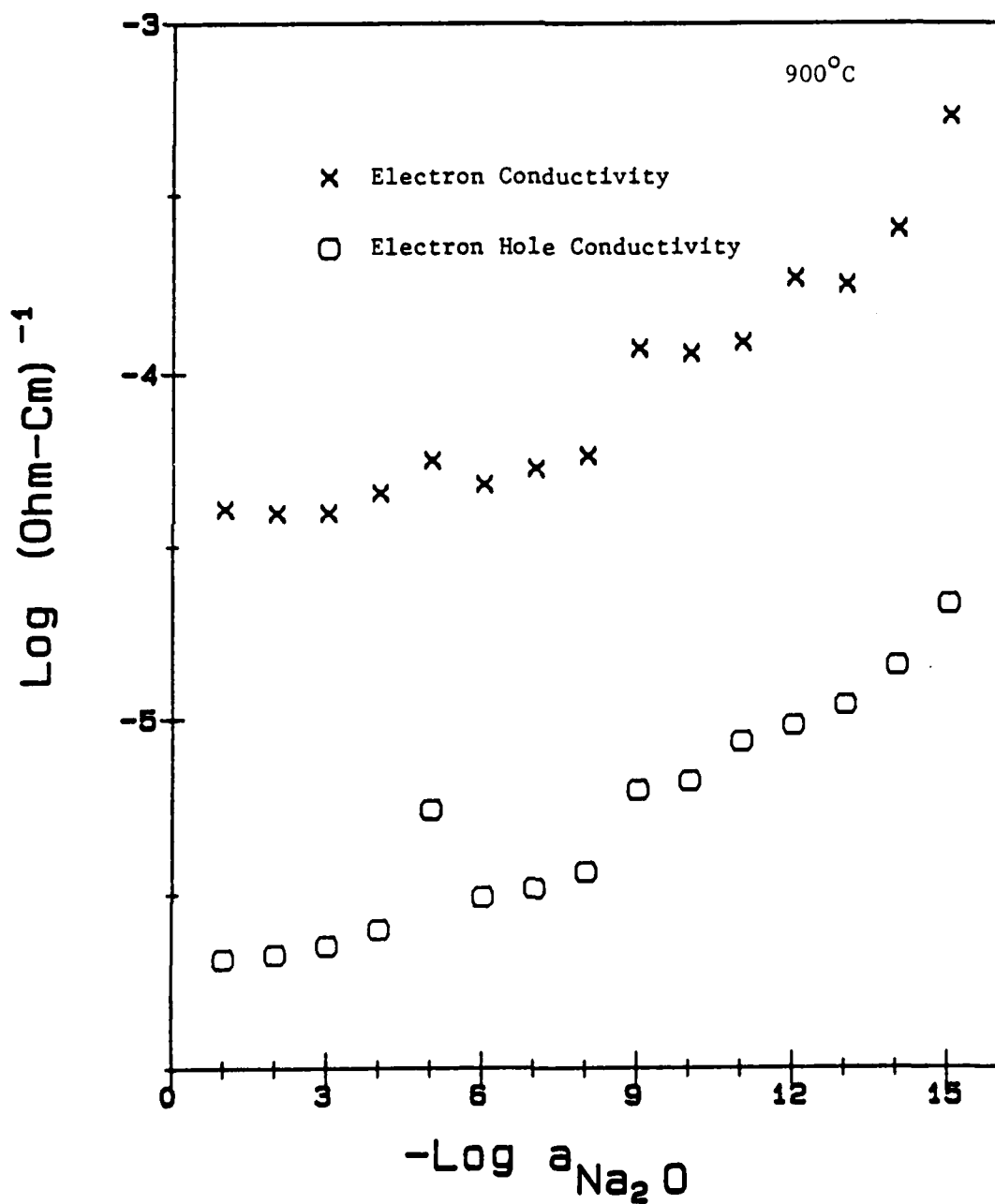


Figure 12. Partial electronic conductivities in a Na₂SO₄ melt containing 10⁻³ m/o α-Fe₂O₃ as a function of Na₂O activity at 1173 K

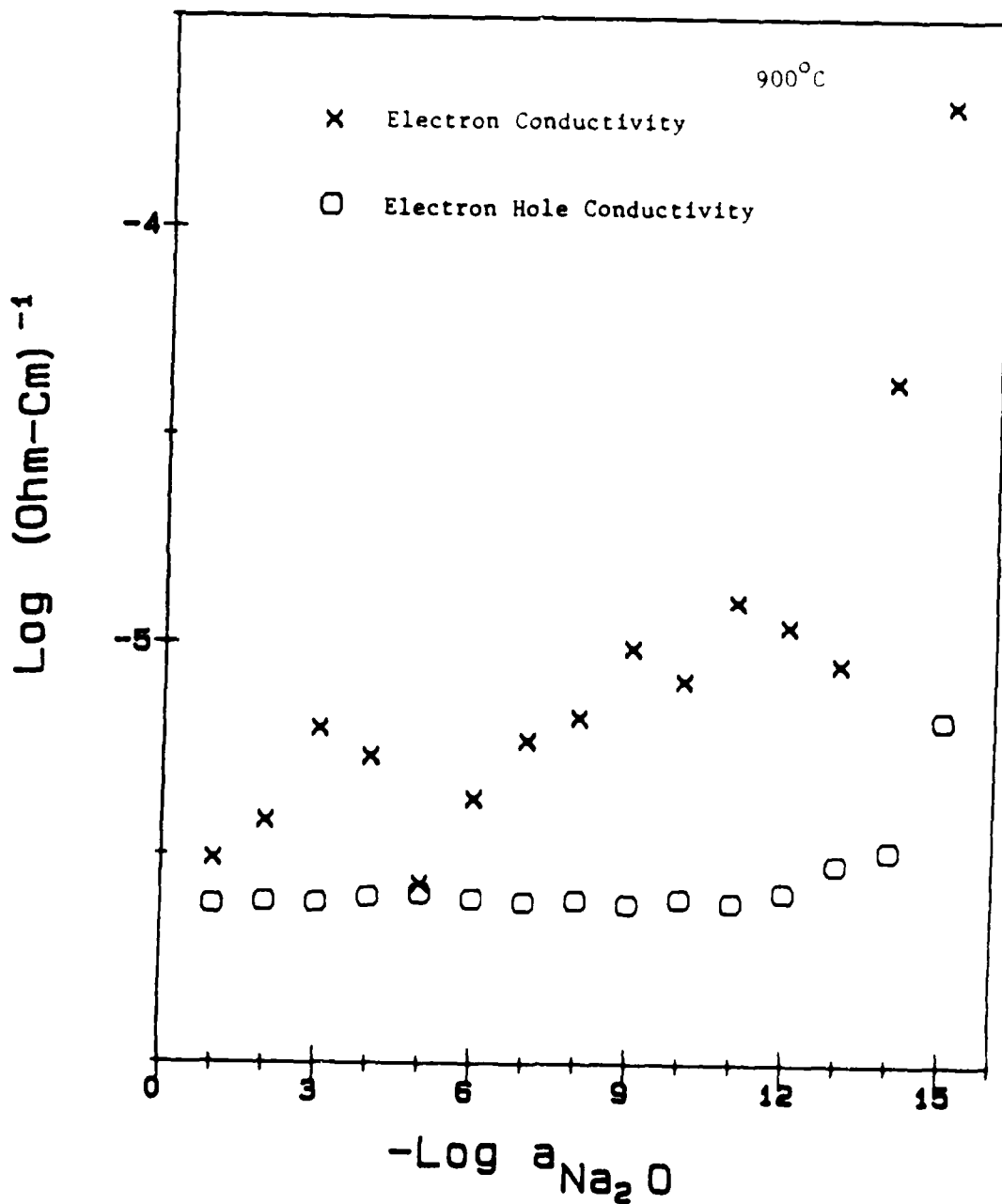


Figure 13. Partial electronic conductivities in Na₂SO₄ melt containing 10⁻² m/o α-Fe₂O₃ as a function of Na₂O activity at 1173 K

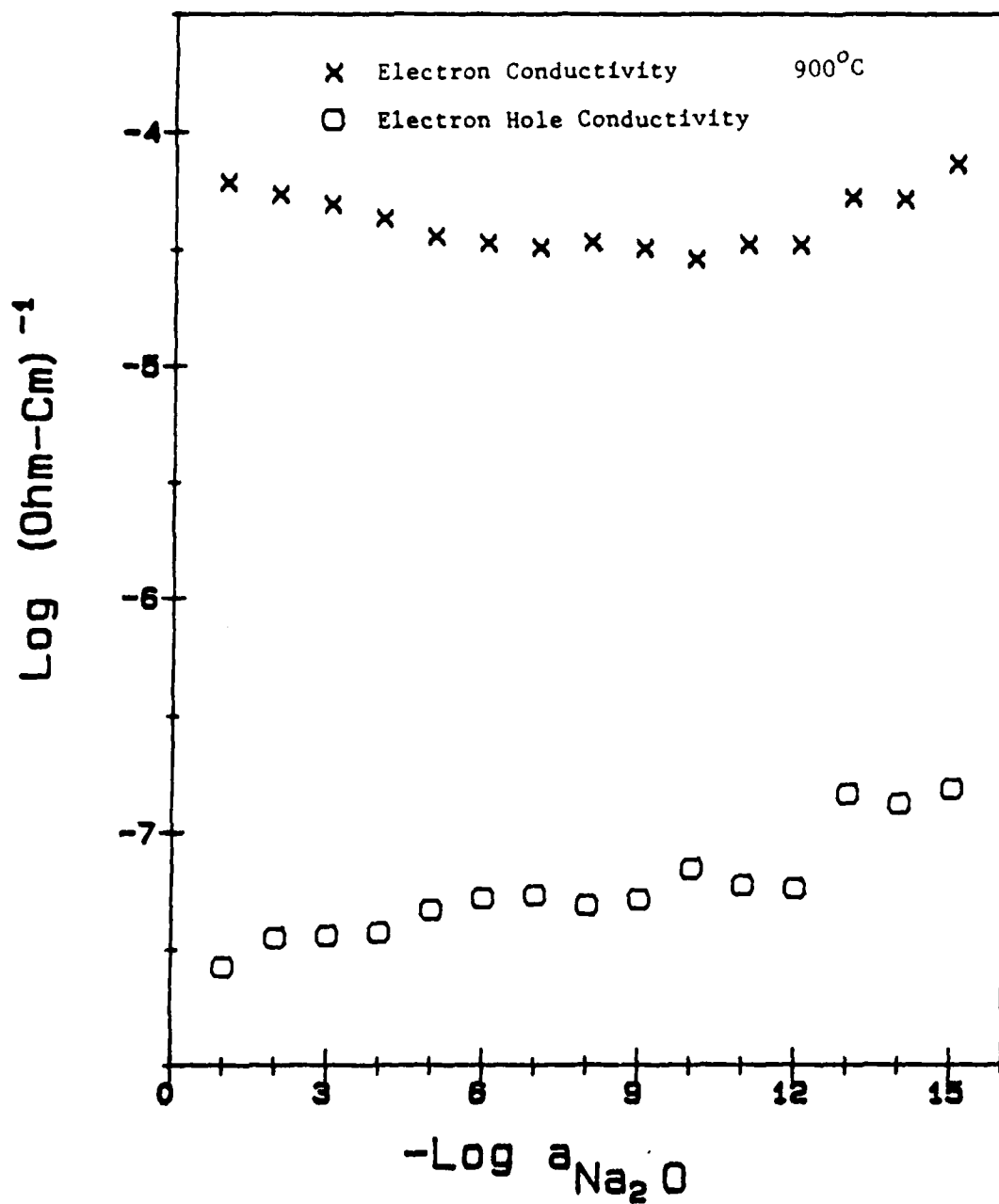


Figure 14. Partial electronic conductivities in a Na_2SO_4 melt containing supersaturated $\alpha\text{-Fe}_2\text{O}_3$ (1 m/o) as a function of Na_2O activity at 1173 K

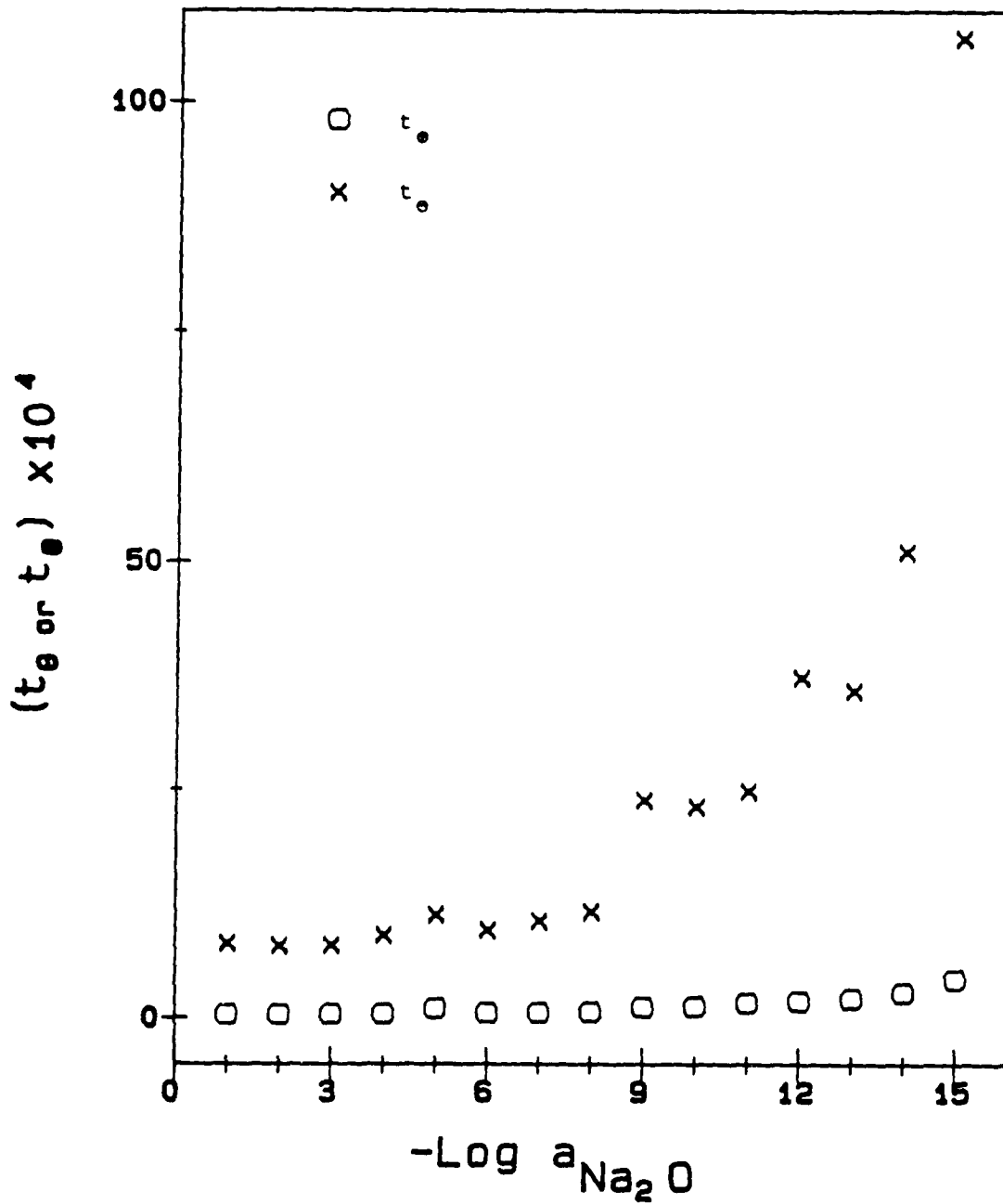


Figure 15. Transport numbers of electronic species in molten Na_2SO_4 with 10^{-3} m/o $\alpha\text{-Fe}_2\text{O}_3$ as a function of Na_2O activity at 1173 K

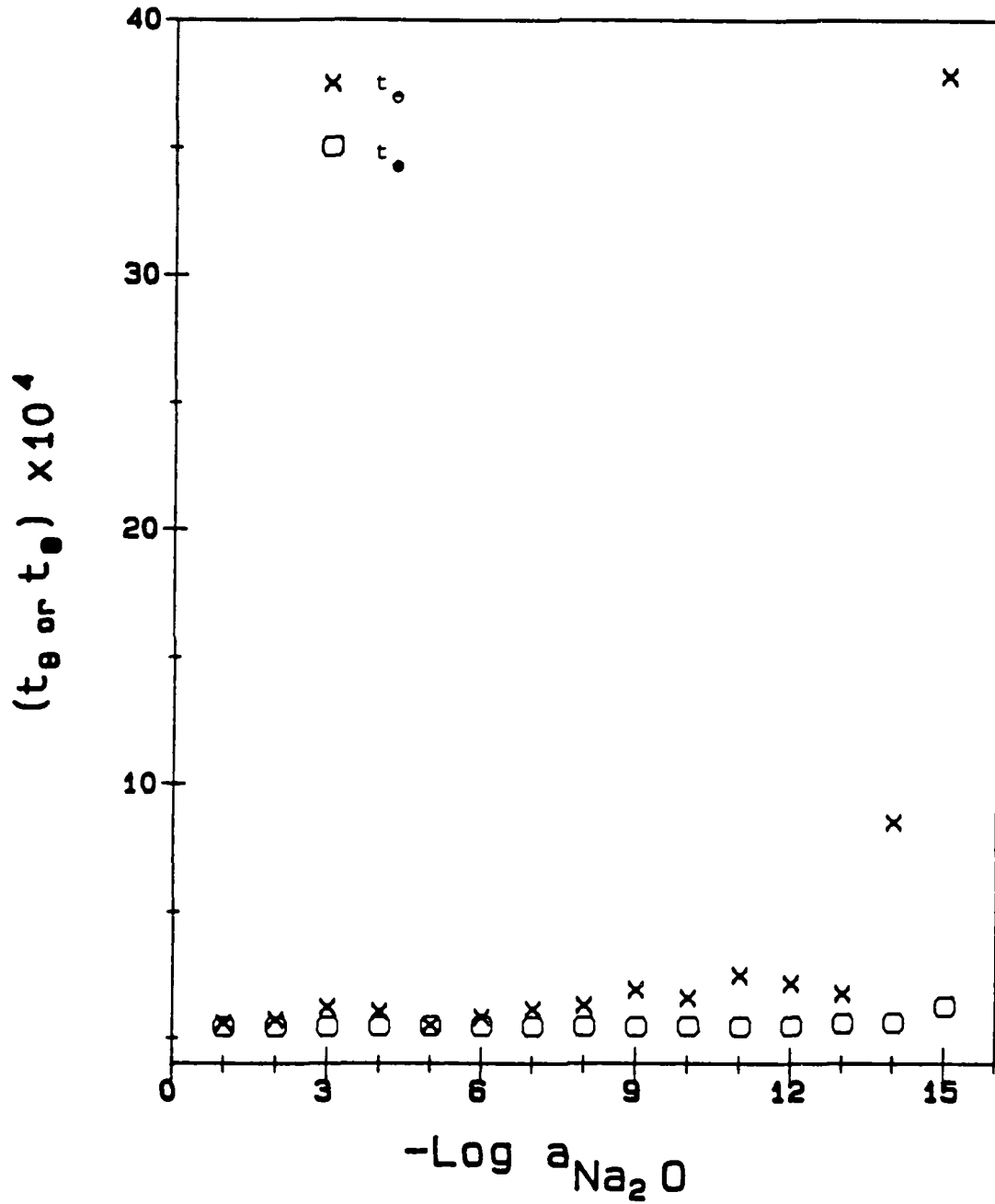


Figure 16. Transport numbers of electronic species in molten Na_2SO_4 with 10^{-2} m/o $\alpha\text{-Fe}_2\text{O}_3$ as a function of Na_2O activity at 1173 K

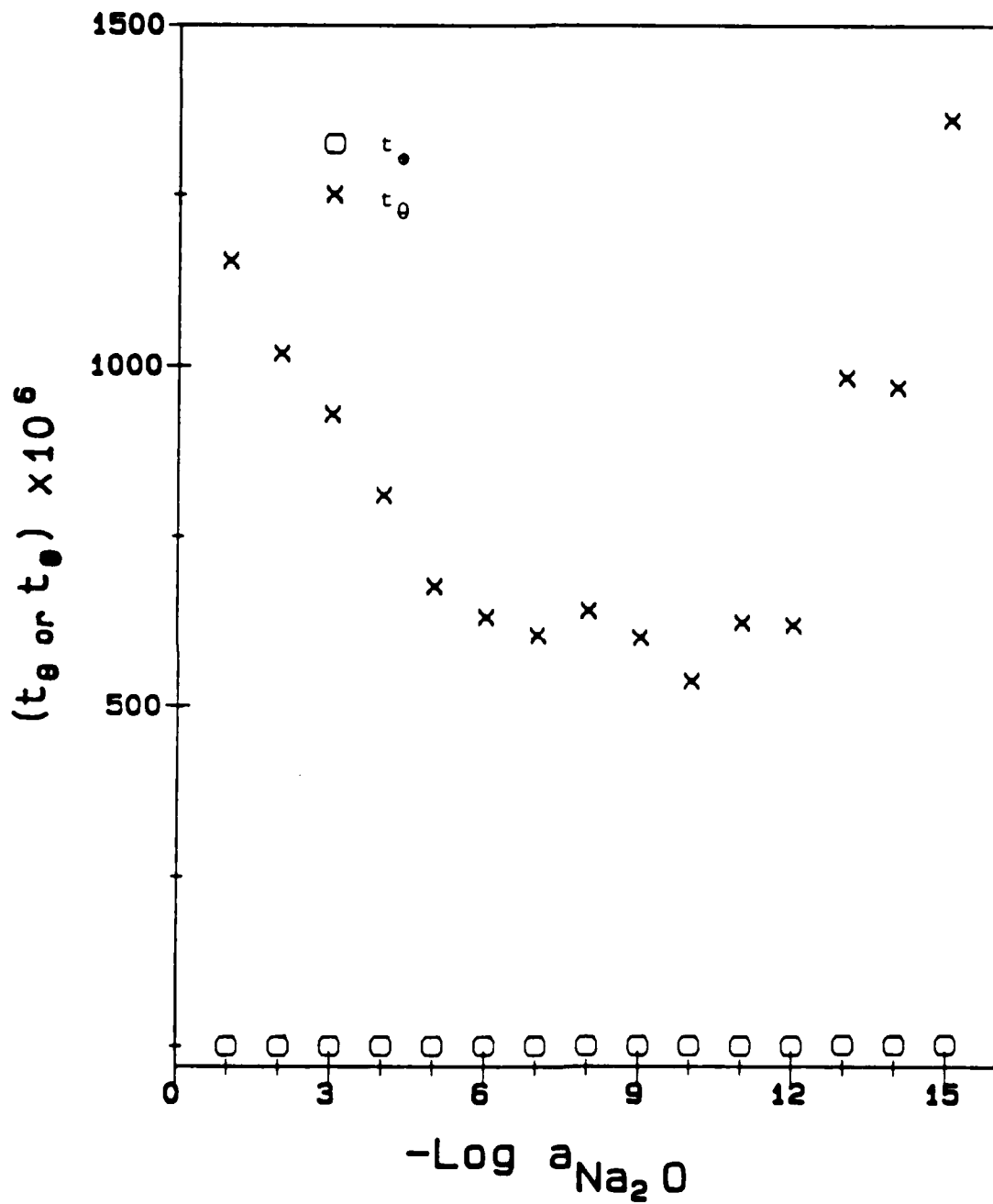


Figure 17. Transpot numbers of electronic species in molten Na_2SO_4 with supersaturated $\alpha\text{-Fe}_2\text{O}_3$ (1 m/o) as a function of Na_2O activity at 1173K

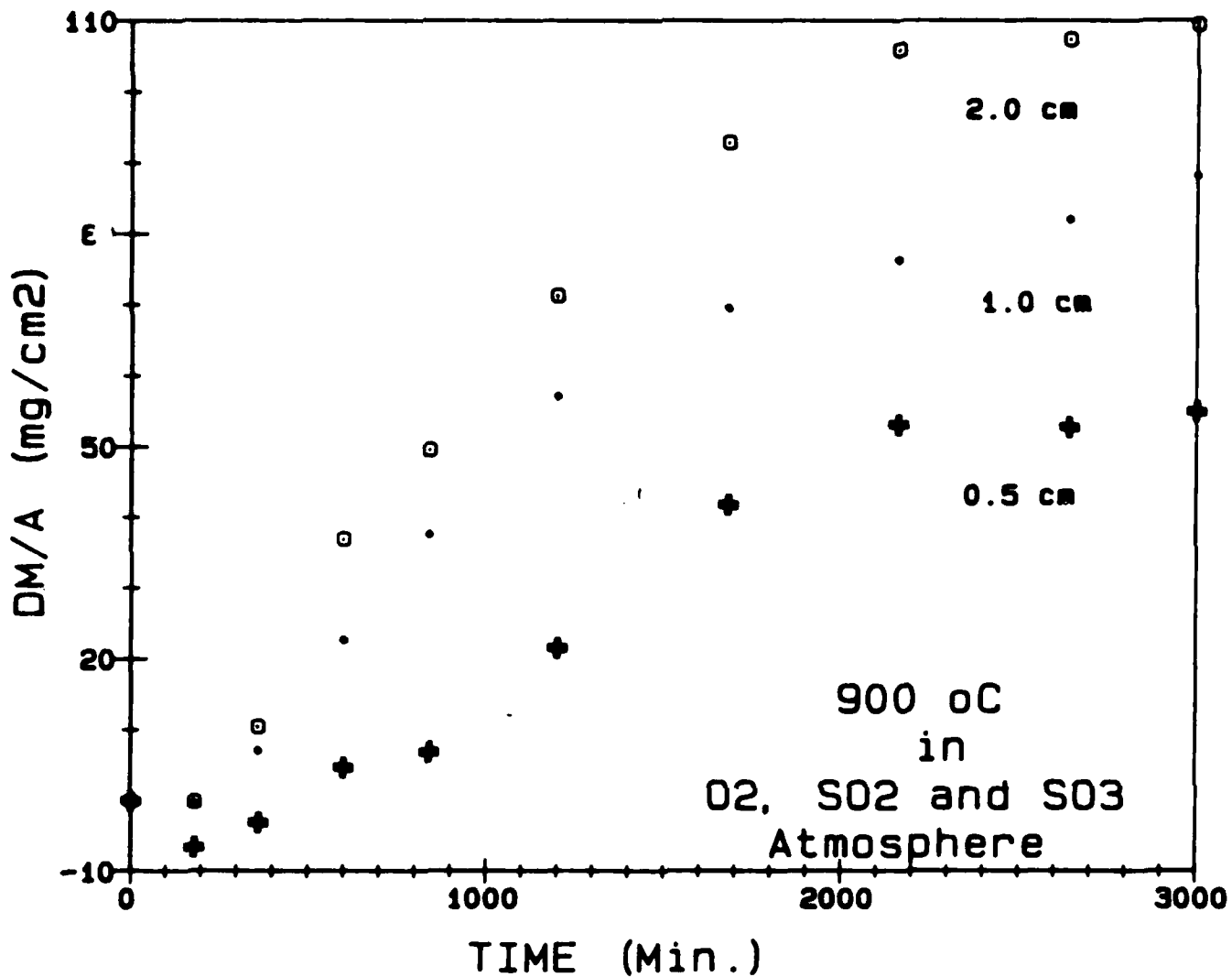


Figure 18. Weight gain vs. time as a function of Na_2O_4 level

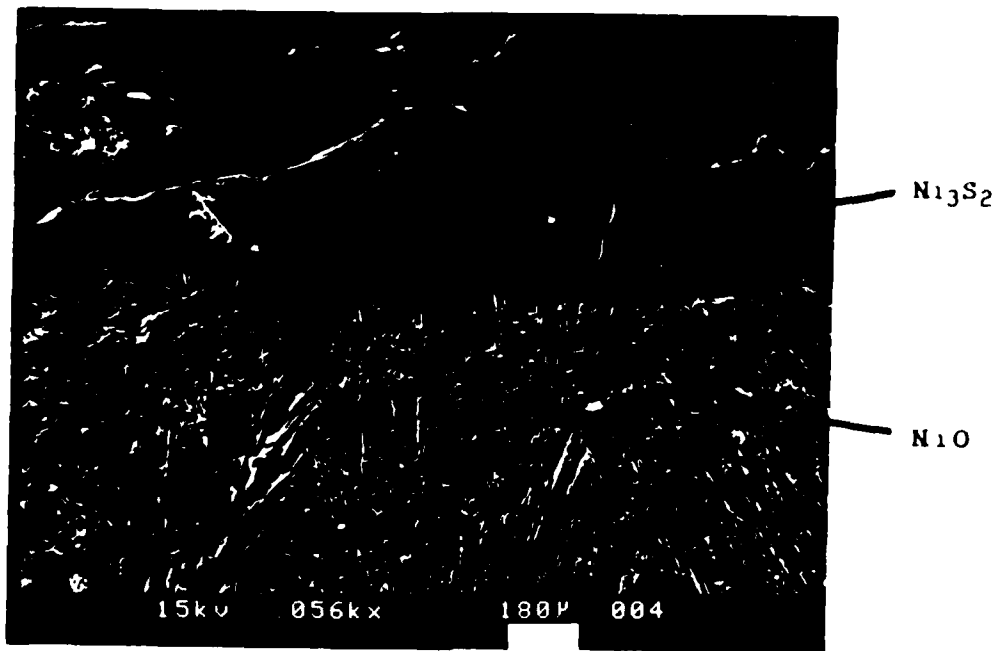


Figure 19. Ni_3S_2 deposit located beneath dense NiO scale

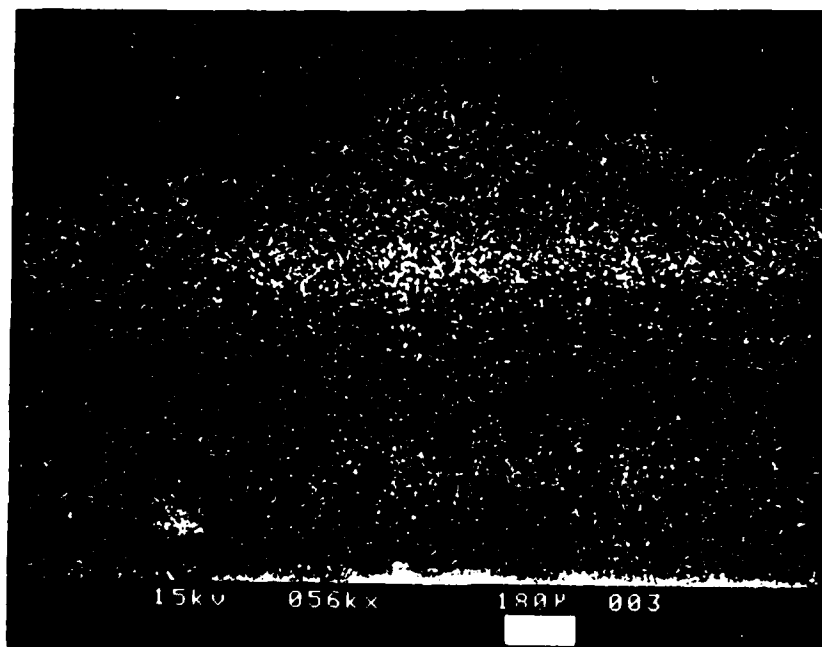


Figure 20. X-ray mapping of the distribution of sulfur

Supplemental Distribution List

Mar 1987

Prof. I.M. Bernstein
Dept. of Metallurgy and Materials Science
Carnegie-Mellon University
Pittsburgh, PA 15213

Prof. H.K. Birnbaum
Dept. of Metallurgy & Mining Eng.
University of Illinois
Urbana, Ill 61801

Prof. H.W. Pickering
Dept. of Materials Science and
Eng.
The Pennsylvania State
University
University Park, PA 16802

Prof. D.J. Duquette
Dept. of Metallurgical Eng.
Rensselaer Polytechnic Inst.
Troy, NY 12181

Prof. J.P. Hirth
Dept. of Metallurgical Eng.
The Ohio State University
Columbus, OH 43210

Prof. H. Leidheiser, Jr.
Center for Coatings and Surface Research
Sinclair Laboratory, Bld. No. 7
Lehigh University
Bethlehem, PA 18015

Dr. M. Kendig
Rockwell International - Science Center
1049 Camino Dos Rios
P.O. Box 1085
Thousand Oaks, CA 91360

Prof. R. A. Rapp
Dept. of Metallurgical Eng.
The Ohio State University
Columbus, OH 43210

Profs. G.H. Meier and F.S. Pettit
Dept. of Metallurgical and
Materials Eng.
University of Pittsburgh
Pittsburgh, PA 15261

Dr. W. C. Moshier
Martin Marietta Laboratories
1450 South Rolling Rd.
Baltimore, MD 21227-3898

Prof. P.J. Moran
Dept. of Materials Science & Eng.
The Johns Hopkins University
Baltimore, MD 21218

Prof. R.P. Wei
Dept. of Mechanical Engineering
and Mechanics
Lehigh University
Bethlehem, PA 18015

Prof. W.H. Hartt
Department of Ocean Engineering
Florida Atlantic University
Boca Raton, Florida 33431

Dr. B.G. Pound
SRI International
333 Ravenswood Ave.
Menlo Park, CA 94025

Prof. C.R. Clayton
Department of Materials Science
& Engineering
State University of New York
Stony Brook
Long Island, New York 11794

Prof. Boris D. Cahan
Dept. of Chemistry
Case Western Reserve Univ.
Cleveland, Ohio 44106

Dr. K. Sadananda
Code 6390
Naval Research Laboratory
Washington, D.C. 20375

Prof. M.E. Orazem
Dept. of Chemical Engineering
University of Virginia
Charlottesville, VA 22901

Mr. T.W. Crooker
Code 6310
Naval Research Laboratory
Washington, D.C. 20375

Prof. G.R. St. Pierre
Dept. of Metallurgical Eng.
The Ohio State University
Columbus, OH 43210

Prof. G. Simkovich
Dept. of Materials Science & Eng.
The Pennsylvania State University
University Park, PA 16802

Dr. E. McCafferty
Code 6310
Naval Research Laboratory
Washington, D. C. 20375

BASIC DISTRIBUTION LIST

Technical and Summary Reports

1985

<u>Organization</u>	<u>Copies</u>	<u>Organization</u>	<u>Copies</u>
Defense Documentation Center Cameron Station Alexandria, VA 22314	12	Naval Air Propulsion Test Center Trenton, NJ 08628 ATTN: Library	1
Office of Naval Research Department of the Navy 800 N. Quincy Street Arlington, VA 22217 Attn: Code 431	3	Naval Construction Battalion Civil Engineering Laboratory Port Hueneme, CA 93043 ATTN: Materials Division	1
Naval Research Laboratory Washington, DC 20375 ATTN: Codes 6000 6300 2627	1 1 1	Naval Electronics Laboratory San Diego, CA 92152 ATTN: Electron Materials Sciences Division	1
Naval Air Development Center Code 606 Warminster, PA 18974 ATTN: Dr. J. DeLuccia	1	Naval Missile Center Materials Consultant Code 3312-1 Point Mugu, CA 92041	1
Commanding Officer Naval Surface Weapons Center White Oak Laboratory Silver Spring, MD 20910 ATTN: Library	1	Commander David W. Taylor Naval Ship Research and Development Center Bethesda, MD 20084	1
Naval Oceans Systems Center San Diego, CA 92132 ATTN: Library	1	Naval Underwater System Center Newport, RI 02840 ATTN: Library	1
Naval Postgraduate School Monterey, CA 93940 ATTN: Mechanical Engineering Department	1	Naval Weapons Center China Lake, CA 93555 ATTN: Library	1
Naval Air Systems Command Washington, DC 20360 ATTN: Code 310A Code 5304B	1 1	NASA Lewis Research Center 21000 Brookpark Road Cleveland, OH 44135 ATTN: Library	1
Naval Sea System Command Washington, DC 20362 ATTN: Code 05R	1	National Bureau of Standards Washington, DC 20234 ATTN: Metals Science and Standards Division Ceramics Glass and Solid State Science Division Fracture and Deformation Div.	1 1 1 1

Naval Facilities Engineering Command Alexandria, VA 22331 ATTN: Code 03	1	Defense Metals and Ceramics Information Center Battelle Memorial Institute 505 King Avenue Columbus, OH 43201	1
Scientific Advisor Commandant of the Marine Corps Washington, DC 20380 ATTN: Code AX	1	Metals and Ceramics Division Oak Ridge National Laboratory P.O. Box X Oak Ridge, TN 37380	1
Army Research Office P. O. Box 12211 Triangle Park, NC 27709 ATTN: Metallurgy & Ceramics Program	1	Los Alamos Scientific Laboratory P.O. Box 1663 Los Alamos, NM 87544 ATTN: Report Librarian	1
Army Materials and Mechanics Research Center Watertown, MA 02172 ATTN: Research Programs Office	1	Argonne National Laboratory Metallurgy Division P.O. Box 229 Lemont, IL 60439	1
Air Force Office of Scientific Research/NE Building 410 Bolling Air Force Base Washington, DC 20332 ATTN: Electronics & Materials Science Directorate	1	Brookhaven National Laboratory Technical Information Division Upton, Long Island New York 11973 ATTN: Research Library	1
		Library Building 50, Room 134 Lawrence Radiation Laboratory Berkeley, CA	1
NASA Headquarters Washington, DC 20546 ATTN: Code RRM	1		

each unless otherwise indicated.

END

6-87

DITIC